

Constraints on the phase diagram of molybdenum from first-principles free-energy calculations

C. Cazorla^{1,2}, D. Alfè^{1,2,3,4}, and M. J. Gillan^{2,3,4}

¹*Department of Earth Sciences, UCL, London, WC1E 6BT, UK*

²*Thomas Young Centre at UCL, London WC1E 6BT, UK*

³*London Centre for Nanotechnology, UCL, London WC1H 0AH, UK*

⁴*Department of Physics and Astronomy, UCL, London WC1E 6BT, UK*

Abstract

We use first-principles techniques to re-examine the suggestion that transitions seen in high- P experiments on Mo are solid-solid transitions from the bcc structure to either the fcc or hcp structures. We confirm that in the harmonic approximation the free energies of fcc and hcp structures become lower than that of bcc at $P > 325$ GPa and T below the melting curve, as reported recently. However, we show that if anharmonic effects are fully included this is no longer true. We calculate fully anharmonic free energies of high- T crystal phases by integration of the thermal average stress with respect to strain as structures are deformed into each other, and also by thermodynamic integration from harmonic reference systems to the fully anharmonic system. Our finding that fcc is thermodynamically less stable than bcc in the relevant high- P /high- T region is supported by comparing the melting curves of the two structures calculated using the first-principles reference-coexistence technique. We present first-principles simulations based on the recently proposed Z method which also support the stability of bcc over fcc.

PACS numbers: 64.10.+h,64.70.D-,64.70.K-,71.15.Pd

I. INTRODUCTION

The past 10 years have seen a lively controversy over the phase diagrams of transition metals at megabar pressures, with the pressure dependence of the melting temperature dT_m/dP from diamond-anvil-cell (DAC) measurements differing greatly from that deduced from shock data and from first-principles calculations (see Fig. 1).¹⁻¹² One suggested resolution of the controversy is that the transition interpreted as melting in some of the DAC experiments may in fact be a solid-solid crystallographic transformation, and in the case of molybdenum this is consistent with the observation of two transitions in shock experiments.^{13,14} This suggestion appeared to be confirmed by recent first-principles work on Mo, which indicated a transition from the low-temperature body-centred-cubic (bcc) structure to a close-packed structure in the appropriate temperature region.^{7,15,16} However, that work relied on two important assumptions, which we examine in detail in this paper. The results we shall present imply that those assumptions and the conclusions drawn from them may be incorrect, so that further work is still needed to resolve the controversy.

DAC measurements have been reported on the melting curves of several transition metals, including Ti, V, Cr, Fe, Co, Ni, Mo, Ta and W.^{3,6,17,18} The measurements extend up to nearly 100 GPa (1 Mbar), and in most cases the increase of melting temperature T_m between ambient pressure and 100 GPa is surprisingly small; in the case of Mo, the increase is only ~ 200 K.^{3,6} These findings are in stark contrast to the melting curves deduced from shock measurements, which are available for Fe, Mo, Ta and W.^{13,14} For Mo, the increase of T_m between ambient and 100 GPa estimated from shock data is ~ 2000 K. Recently, density functional theory (DFT) calculations of the melting curves of Mo and Ta have been reported.^{1,2,7,9,19} The DFT predictions are expected to be reliable, because it is well known that DFT, without any adjustable parameters, gives excellent results for a wide range of properties of transition metals, including cold compression curves up to ~ 300 GPa,^{1,2,20,21} Hugoniot $P(V)$ curves,^{4,22,23} phonon dispersion relations (and their pressure dependence, in the case of Fe),^{1,2,24-26} and low-temperature phase boundaries.²⁷ Furthermore, techniques for calculating melting curves using DFT have become firmly established over the past 10 years and more, and are known to give accurate results.²⁸⁻³⁴ The DFT results for $T_m(P)$ of Mo and Ta lend support to the correctness of the melting curves deduced from shock data.^{1,2,7,9}

It has become clear very recently that experimental difficulties may have led to a sub-

stantial underestimate of high- P melting temperatures in earlier DAC measurements. The work of Dewaele *et al.*¹⁰ indicates that formation of metal carbide by chemical reaction between the diamond and the metal sample can be a major problem. Their work also shows that difficulties in the pyrometric measurement of temperature can also lead to substantial underestimates of T_m . In the case of Ta, their measurements give a melting curve that is well above those given by earlier DAC experiments and is fairly close to (though systematically lower than) the predictions from DFT. Nevertheless, in the case of Mo, the occurrence of two breaks in the shock data seems to leave little doubt that there is a transition from the low- T bcc structure to an unidentified high- T crystal structure, followed by the melting of the latter. The T and P of the lower transition (3500 K and 200 GPa) lie close to the natural extrapolation of the $T(P)$ boundary identified as melting in the older DAC experiments. This suggests that this boundary is associated with a bcc-solid transition. Even in the case of Ta, recent evidence based on DFT calculations⁹ indicates that a bcc-solid transition is implicated in earlier DAC attempts to detect high- P melting.

To substantiate the picture of a bcc-solid transition followed by a melting transition, it is necessary to show that another crystal structure becomes thermodynamically more stable than bcc at high temperatures, and to identify this structure. This was the aim of the recent DFT work on Mo by Belonoshko *et al.*⁷ They showed that, in the quasiharmonic approximation, the Gibbs free energy of the fcc structure is lower than that of bcc over a substantial high- P /high- T region of the phase diagram below the bcc melting curve. The fcc structure becomes harmonically unstable (there are imaginary phonon frequencies) for $P < 350$ GPa, but extrapolation of the predicted bcc-fcc phase boundary passes quite close to the (P, T) of the lower shock transition. The quasiharmonic calculations on the bcc and fcc free energies were independently confirmed by two subsequent papers.^{15,16} As independent evidence that fcc is more stable than bcc at high T , Belonoshko *et al.*⁷ used the Z method^{35,36} to calculate the melting curve of fcc Mo. (The Z method employs observations of spontaneous melting of the superheated solid in constant-energy molecular dynamics simulations to determine points on the melting curve.) They found that the fcc melting curve lies above the bcc melting curve, thus appearing to confirm that the free energy of fcc is lower than bcc. However, we note the two important assumptions made here: first, that anharmonic contributions to the free energies of high- T bcc and fcc Mo can be neglected; and second, that the first-principles statistical-mechanical techniques that were employed

have the precision needed to distinguish between the possibly rather similar melting curves of bcc and other structures. There is also the question of whether fcc can remain vibrationally stable at high T in the region $P < 350$ GPa, where the harmonic phonons are unstable. These are the issues addressed in the present paper.

We use two methods here for comparing the free energies of the bcc and other crystal structures, and both methods fully include anharmonicity. The other structures we examine are fcc and hexagonal-close-packed (hcp). The first method uses the fact that the free energy difference between two systems that differ only by a finite strain can be obtained by integrating the thermal average stress with respect to strain.^{37,38} We use this idea to obtain the free energy difference between fcc and bcc, which can be transformed into each other by a continuous strain along the Bain path (BP). The second method employs thermodynamic integration (TI) from a harmonic reference system to the fully anharmonic system described by DFT. This is essentially the same method as we employed in earlier work on Fe.^{4,29,39} As further ways of probing the possible thermodynamic stability of the fcc structure, we have re-examined the melting curve of fcc Mo, using the reference coexistence technique employed in some of our earlier work,^{33,34,40,41} and we have also performed our own first-principles Z -method calculations on the melting of bcc and fcc Mo. All the results point to the conclusion that none of the other structures is thermodynamically more stable than bcc at high T .

The rest of the paper is organised as follows. In Sec. II, we summarise briefly the technical details of the DFT methods employed in all the calculations, and we then present our results for the harmonic dispersion relations of the bcc, fcc and hcp structures over a wide range of P ; we note the pressure thresholds below which the fcc and hcp structures become harmonically unstable. In the same Section, we report our results for the harmonic free energies, and hence the predicted phase boundaries separating the different structures. Sec. III presents our results on the vibrational, elastic and thermodynamic stability of the different structures, including our Bain-path calculations of the free energy differences between fcc and bcc. Our calculations of the anharmonic contributions to the free energy, and the effect of these contributions on the phase boundaries are presented in Sec. IV. Our reference coexistence calculations of the fcc melting curve and the comparison with the bcc melting curve obtained already by the same technique are outlined in Sec. V, where we also present our new Z -method calculations. Finally, we draw all the results together in Sec. VI, and suggest what

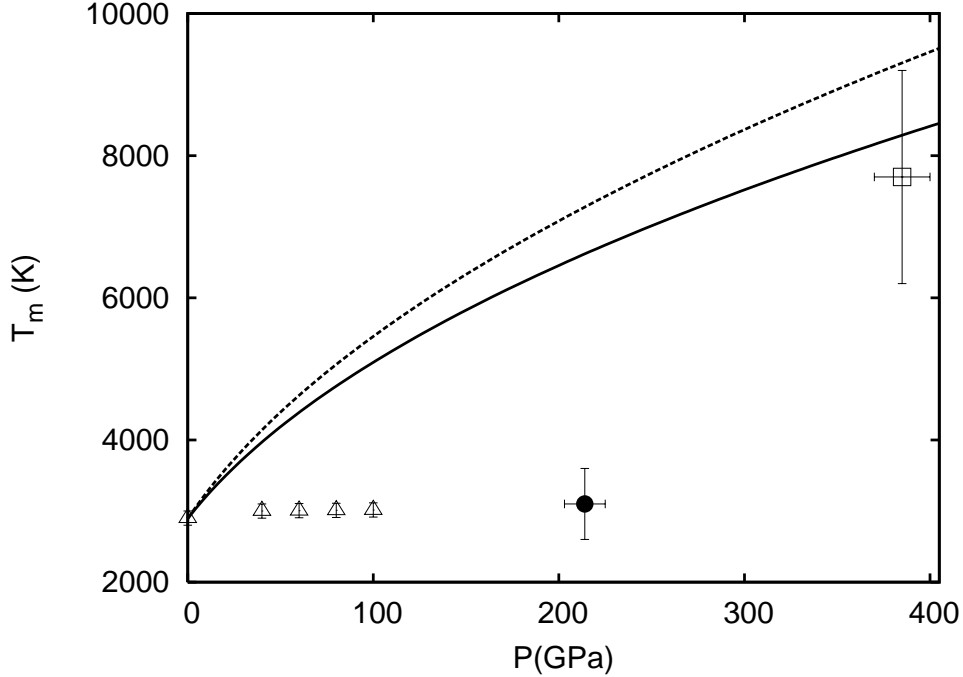


FIG. 1: Points on the solid-liquid boundary of Mo as observed in DAC (\triangle [3]) and shock wave (\square [13]) experiments. The shock wave datum (\bullet [13]) obtained at low- P has been interpreted as a solid-solid phase transition. Lines represent theoretical predictions of the melting curve of bcc Mo by Cazorla *et al.* (solid line [1]) and Belonoshko *et al.* (dashed line [7]).

future investigations might help to resolve the controversies over the phase diagram of Mo and other transition metals.

II. HARMONIC CALCULATIONS

A. DFT techniques

All calculations were done using the projector augmented wave version of DFT as implemented in the VASP package.^{42,43} All atomic states up to and including 4s were treated as core states, with 4p and all higher states being valence states. We used the PBE form of generalised gradient approximation to the exchange-correlation functional.⁴⁴ An energy cut-off of 224.6 eV was used throughout; the adequacy of this value was shown in a previous work where we performed extensive numerical convergence tests.¹ Dense Monkhorst-Pack grids⁴⁵ were used for electronic k -point sampling in static perfect lattice calculations, to guarantee

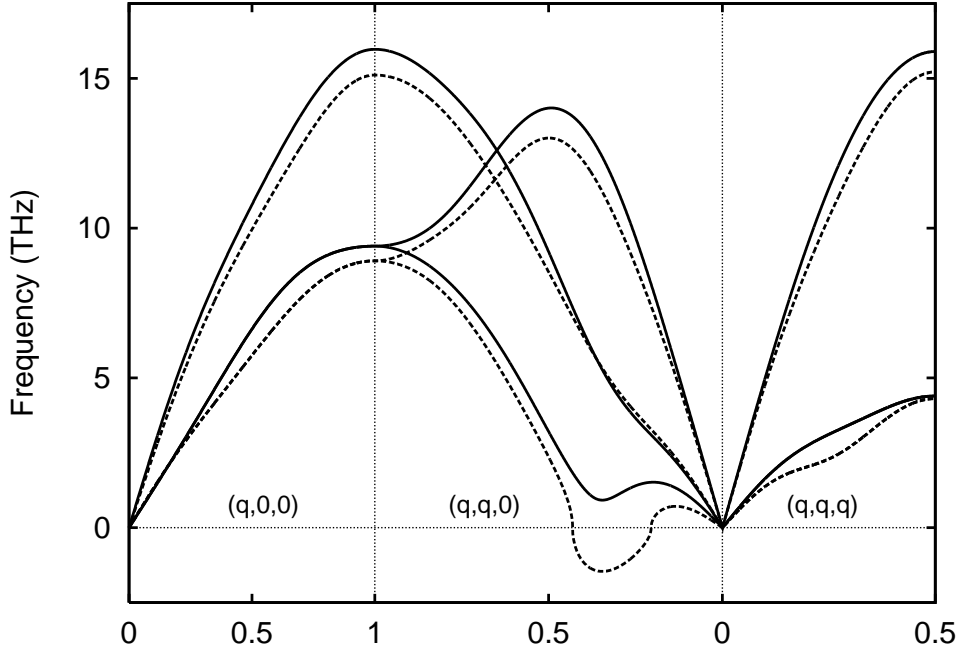


FIG. 2: *Ab initio* vibrational phonon frequencies of Mo in the fcc structure calculated at volumes $V = 9.64 \text{ \AA}^3/\text{atom}$ ($P = 328 \text{ GPa}$, solid line) and $V = 10.19 \text{ \AA}^3/\text{atom}$ ($P = 265 \text{ GPa}$, dashed line).

convergence of the total energy to better than 1 meV/atom. Thermal excitation of electrons was included via the finite- T version of DFT originally developed by Mermin.^{46,47} Phonon frequencies in our calculations were obtained by the small-displacement method^{48,49} using large supercells. For molecular dynamics (MD) simulations, we used the Born-Oppenheimer scheme where the self-consistent ground state is recalculated at each MD time-step. These simulations were performed in the microcanonical (N, V, E) and canonical (N, V, T) ensembles; temperatures in (N, V, T) simulations were maintained using Nosé thermostats. Values of the technical parameters (duration of the MD runs, \mathbf{k} -point grids, number of atoms, etc.) will be presented together with the results.

B. Harmonic free energies and phase boundaries

It is convenient to represent the total Helmholtz free energy $F(V, T)$ of the system at volume V and temperature T as the sum of three parts:⁴⁷

$$F(V, T) = F_p(V, T) + F_h(V, T) + F_a(V, T). \quad (1)$$

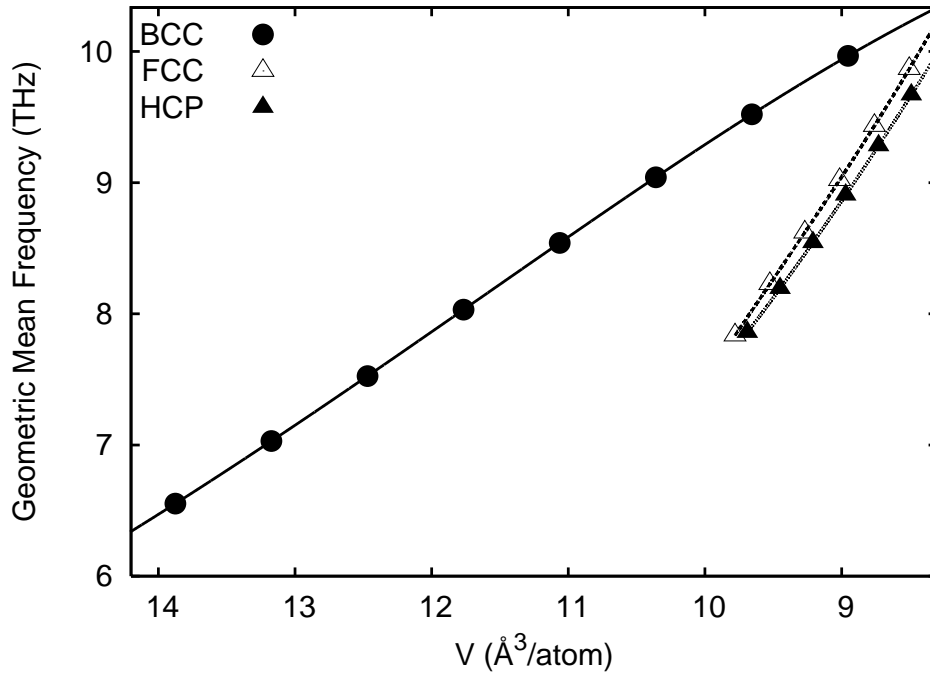


FIG. 3: Geometric mean frequency $\bar{\omega}$ of Mo in the bcc, fcc and hcp structures as a function of volume. Symbols represent states at which the calculations have been carried out and the lines are guides to the eye.

Here, F_p is the Helmholtz free energy of the static perfect lattice: it is a *free* energy, because we include thermal electronic excitations.^{46,47} The second term F_h is the free energy due to lattice vibrations, calculated in the harmonic approximation. The remainder F_a accounts for anharmonicity; we ignore F_a here, but show how to compute it in Sec. IV.

The calculation of $F_p(V, T)$ is completely standard. It is known from previous work that at $T = 0$ K and pressures $P < 660$ GPa the most stable phase of Mo is bcc.^{7,27} At higher compressions, Mo stabilizes in the double hexagonal closed-packed (dhcp) structure as recently shown by Belonoshko *et al.* (see Fig. 1 of Ref. [7]) and confirmed in our own calculations. Since we focus here on pressures $P < 600$ GPa, we have computed $F_p(V, T)$ on a grid of (V, T) points for the bcc, fcc and hcp structures. This grid spans the ranges $8.25 \leq V \leq 15.55 \text{ \AA}^3/\text{atom}$ and $0 \leq T \leq 10000$ K, with state points taken at intervals of $0.5 \text{ \AA}^3/\text{atom}$ and 500 K, respectively. We then fit the $F_p(V, T)$ results obtained at fixed T

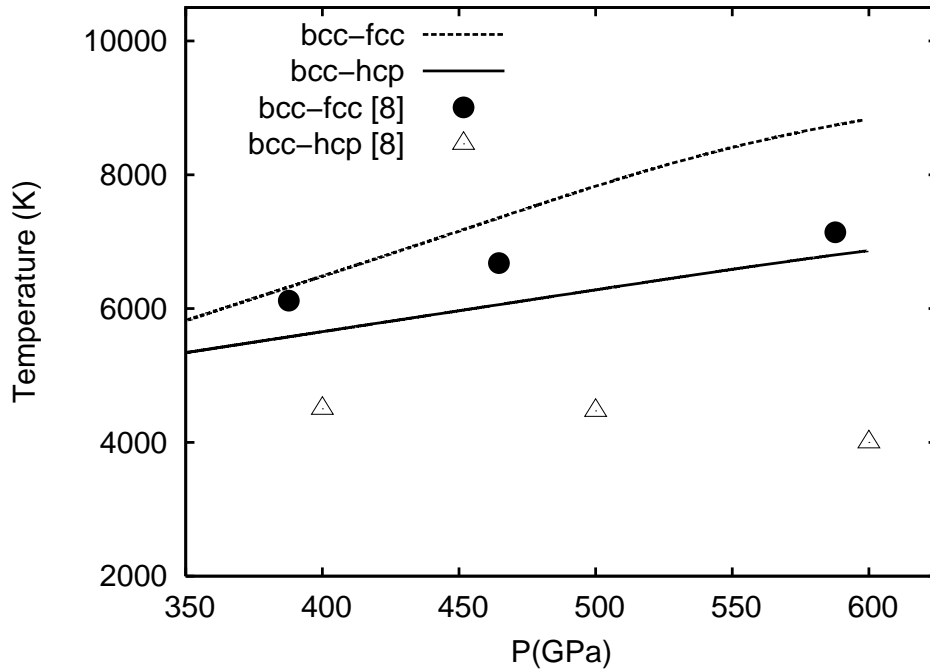


FIG. 4: Solid-solid phase boundaries in Mo at high P and high T as obtained with first-principles harmonic free-energy calculations. Results obtained by Belonoshko *et al.* [7] are shown for comparison.

to a third-order Birch-Murnaghan equation⁵⁰ of the form

$$\begin{aligned}
 F_p(V, T) = E_0 + \frac{3}{2} V_0 K_0 \left[-\frac{\chi}{2} \left(\frac{V_0}{V} \right)^2 + \frac{3}{4} (1 + 2\chi) \left(\frac{V_0}{V} \right)^{4/3} \right. \\
 \left. - \frac{3}{2} (1 + \chi) \left(\frac{V_0}{V} \right)^{2/3} + \frac{1}{2} \left(\chi + \frac{3}{2} \right) \right], \quad (2)
 \end{aligned}$$

where E_0 and $K_0 = -V_0 d^2 E / dV^2$ are the values of the energy and the bulk modulus at equilibrium volume V_0 , respectively, $\chi = \frac{3}{4} (4 - K'_0)$ and $K'_0 = [\partial K / \partial P]$, with derivatives evaluated at zero pressure. Finally, the dependence of parameters E_0 , K_0 , V_0 and K'_0 on T is fitted to 4-th order polynomial expressions.

We obtain the harmonic phonon frequencies $\omega_{\mathbf{q},s}$ by diagonalising the dynamical matrix, which is the spatial Fourier transform of the force-constant matrix. Our calculations of the latter by the small-displacement method,^{48,49} used large supercells of 216 atoms ($4 \times 4 \times 4$ k -point grid) for the bcc and fcc structures and 200 atoms for hcp ($4 \times 4 \times 3$ k -point grid). We performed extensive tests for Mo in the bcc structure which showed that these parameters¹ guarantee F_h values converged to less than 1 meV/atom; these parameters are assumed to be

equally adequate for the fcc and hcp structures. In principle, the force-constant matrix and the frequencies $\omega_{\mathbf{q},s}$ depend on the electronic temperature, but we ignore this dependence here. Phonon calculations performed with an electronic T equal to 2000 and 5000 K provide F_h results that agree within 1 meV/atom, so we used $T = 2000$ K in all the $\omega_{\mathbf{q},s}$ calculations.

The phonons are stable for bcc over the entire range $0 < P < 600$ GPa, as is known from previous work^{7,16}. However, the phonons for fcc and hcp are stable only above a threshold pressure P_{th} . To illustrate this, we show in Fig. 2 the fcc phonon frequencies at $V = 9.64 \text{ \AA}^3/\text{atom}$ ($P = 328$ GPa) and $V = 10.19 \text{ \AA}^3/\text{atom}$ ($P = 265$ GPa). We see that the phonon instability first occurs at a finite wavevector, which we estimate as $\mathbf{q}_{inst} = (2\pi/a_0)(1/4, 1/4, 0)$. We find threshold pressures of $P_{th} = 310$ and 325 GPa for the fcc ($V = 9.78 \text{ \AA}^3/\text{atom}$) and hcp ($V = 9.69 \text{ \AA}^3/\text{atom}$) structures.

When calculating the harmonic vibrational free energy $F_h(V, T)$, we use the classical expression:

$$F_h(V, T) = 3k_B T \ln(\hbar\bar{\omega}/k_B T), \quad (3)$$

where $\bar{\omega}$ is the geometric mean frequency, defined by:

$$N_{\mathbf{q},s}^{-1} \sum_{\mathbf{q},s} \ln(\omega_{\mathbf{q},s}/\bar{\omega}) = 1, \quad (4)$$

with the sum going over all $N_{\mathbf{q},s}$ phonon modes (wavevector \mathbf{q} , branch s) in the first Brillouin zone. This classical formula for F_h is valid at temperatures well above the Debye temperature, which for Mo is around 400 K at equilibrium. We have checked that even at $T = 1000$ K the difference between the F_h values obtained with the classical and quantum formulas is less than 1 meV/atom, so our choice does not affect the accuracy of the results.

We show the calculated mean frequencies $\bar{\omega}$ for all the structures in Fig. 3. Comparison of the $\bar{\omega}$ values indicates that harmonic contributions to the free-energy tend to stabilize the fcc and hcp structures over bcc, since $\bar{\omega}^{hcp} < \bar{\omega}^{bcc}$ and $\bar{\omega}^{fcc} < \bar{\omega}^{bcc}$ in the V range studied. The stabilisation is slightly greater for hcp than for fcc.

We fit the dependence of the quantity $\ln(\hbar\bar{\omega})$ on V to a 3rd-order polynomial for all the structures in order to know the value of F_h at any (V, T) thermodynamic state using formula (3). From the harmonic free energies $F'(V, T) = F_p(V, T) + F_h(V, T)$, we have determined the transition bcc-fcc and bcc-hcp pressures at each temperature using the double-tangent construction. The phase boundaries given by these calculations are shown in Fig. 4, where we also indicate the harmonic phase boundaries from the calculations by Belonoshko

*et al.*⁷ (The boundaries given by the very recent quasiharmonic calculations of Zeng *et al.*¹⁶ are similar.) In fact, there are some discrepancies. For instance, those calculated by Belonoshko *et al.* lie at somewhat lower T than ours, and the slopes of the two harmonic bcc-hcp boundaries differ in sign. Despite these differences, we agree with Belonoshko *et al.* that in the harmonic approximation the stable high- P /high- T structure of Mo is hcp.

III. VIBRATIONAL, ELASTIC AND THERMODYNAMIC STABILITY

Do the phase boundaries predicted by harmonic theory have anything to do with the transitions seen in DAC and shock experiments? If they do, then the simplest hypothesis is that these transitions lie on a continuation of the predicted boundaries. But in order for this to be true, several conditions must be satisfied. First, since the lower shock transition occurs at $P = 220$ GPa, which is far below the harmonic stability limit for both fcc and hcp, the system must somehow be vibrationally stabilised, presumably by anharmonic effects. Second, the system must remain elastically stable at pressures $P < 220$ GPa, i.e. small, arbitrary volume-conserving strains must not cause the free energy to decrease. Third, the crystal structures must have lower free energies than bcc. Vibrational stability can be tested by straightforward first-principles MD simulations, as has been shown in our earlier work on high- P /high- T bcc Fe,³⁹ and in recent work by Asker *et al.* on low- P fcc Mo;⁵¹ we report tests here for fcc Mo. The strain dependence of free energy can be also probed by MD calculations in which the thermal average stress is monitored. For the case of fcc, calculation of stress as a function of strain along the Bain path also allows us to test its thermodynamic stability.

A. Vibrational stability

When we say that a crystal in thermal equilibrium is vibrationally stable, we mean that the thermal average position of each atom remains centred on its perfect-lattice site, and does not acquire a permanent deviation away from that site. To test this, it is convenient to use the so-called position correlation function $p(t)$, defined by:³⁹

$$p(t) = \langle (\mathbf{r}_i(t + t_0) - \mathbf{R}_i^0) \cdot (\mathbf{r}_i(t_0) - \mathbf{R}_i^0) \rangle, \quad (5)$$

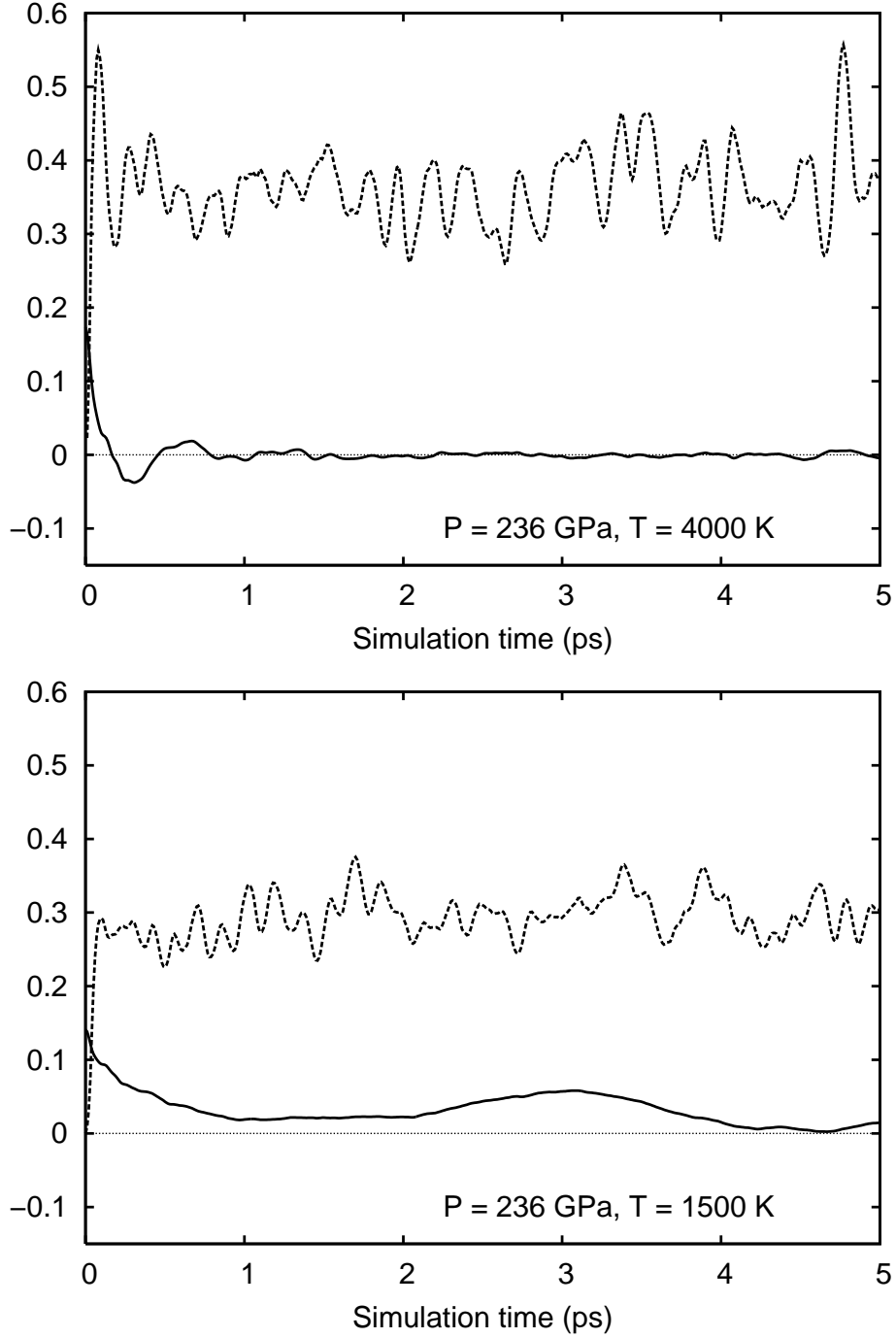


FIG. 5: Calculated mean squared displacement $\Delta r(t)^2$ (dashed line) and position correlation function $p(t)$ (solid line) of Mo in the fcc structure as a function of time. The simulations were performed at two different temperatures and fixed volume $V = 10.50 \text{ \AA}^3/\text{atom}$. The value of functions $\Delta r(t)^2$ and $p(t)$ is in units of \AA^2 .

where $\mathbf{r}_i(t)$ is the position of atom i at time t , \mathbf{R}_i^0 is the perfect-lattice position of the atom, t_0 is an arbitrary time origin, and $\langle \cdot \rangle$ denotes the thermal average. In practice, the thermal average is performed by averaging over t_0 and over atoms. At $t = 0$, $p(t)$ is simply the vibrational mean square displacement. The crystal is vibrationally stable if $p(t \rightarrow \infty) = 0$, because the vibrational displacements at widely separated times become uncorrelated. But if atoms acquire a permanent vibrational displacement, then $p(t \rightarrow \infty)$ becomes non-zero. The characteristic behaviour of $p(t)$ in a vibrationally unstable crystal can be seen in our earlier work on high- P /high- T Fe in the bcc structure.³⁹ For this test to work, the atoms must not diffuse from one site to another, and we routinely test for lack of diffusion by monitoring the time-dependent mean square displacement $\Delta r(t)^2 \equiv \langle |\mathbf{r}_i(t + t_0) - \mathbf{r}_i(t_0)|^2 \rangle$, which, in the absence of diffusion, goes to a constant equal to twice the vibrational mean square displacement in the limit $t \rightarrow \infty$.

We have performed a set of first-principles MD simulations on Mo in the bcc and fcc structures at a wide range of thermodynamic states. A typical MD run consisted of 10^4 steps performed with a time-step of 1 fs, with the first 5 ps allowed for equilibration, and only the last 5 ps used to accumulate statistical averages. The simulation cell contained 125 particles for both fcc and bcc structures and Γ -point electronic k -point sampling was used.

The MD runs were carried out for a total of 20 state points, spanning the ranges $200 \leq P \leq 600$ GPa and $1500 \leq T \leq 10500$ K. In Fig. 5, we show the mean squared displacement $\Delta r(t)^2$ and the position correlation function $p(t)$ calculated for fcc Mo at volume $V = 10.50 \text{ \AA}^3/\text{atom}$ and $T = 1500$ and 4000 K. At the lower T , the system is vibrationally unstable, as shown by the long- t behaviour of $p(t)$. Clearly, atomic liquid-like diffusion does not occur as shown by the fluctuation of $\Delta r(t)^2$ about a constant value at long t . Since these MD simulations are very demanding, we did not attempt to estimate an accurate boundary in the $P - T$ plane separating stable and unstable states of the fcc structure. Nevertheless, we can say that vibrational instability was not observed in our simulations at temperatures $T > 3000$ K and pressures below $P_{\text{th}} = 310$ GPa. The recent work of Asker *et al.*⁵¹ using techniques similar to those used here, showed that even at $P \sim 0$ GPa fcc Mo is vibrationally stable for $T \geq 3000$ K.

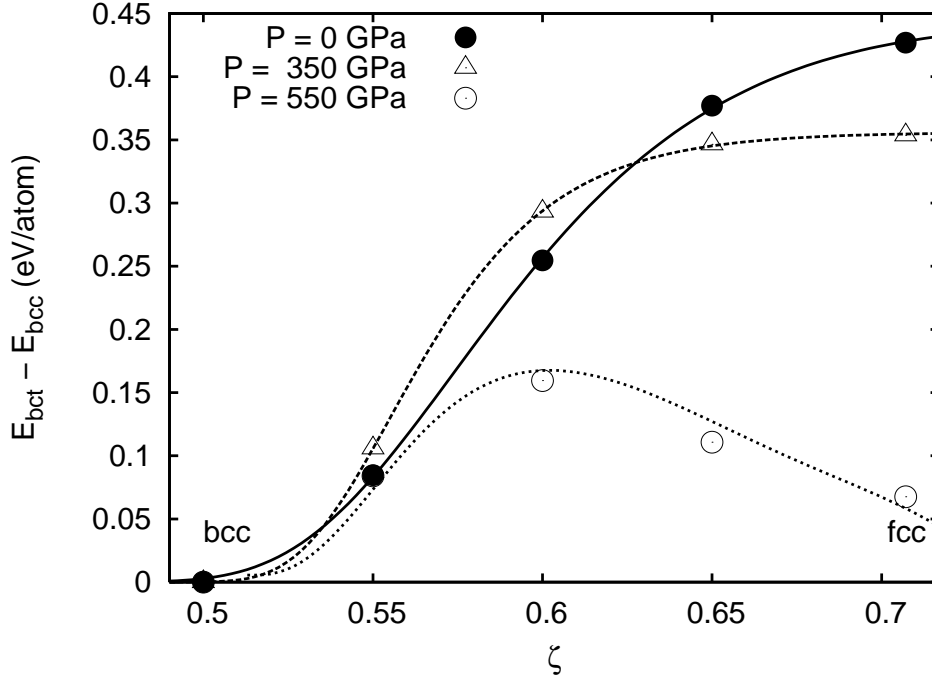


FIG. 6: *Ab initio* free energy calculations performed along the Bain path at zero temperature. Energy differences are represented with symbols, and lines are guides to the eye.

B. Elastic and thermodynamic stability

The elements of the stress tensor $\sigma_{\alpha\beta}$ in a thermal-equilibrium system can be defined as $\sigma_{\alpha\beta} = V^{-1}(\partial F / \partial \epsilon_{\alpha\beta})_T$, where F is the Helmholtz free energy, $\epsilon_{\alpha\beta}$ is the strain tensor, and V is the volume. This relation can be integrated to obtain the difference of free energy between two states that differ by a finite homogeneous strain.^{37,38} The bcc and fcc structures can be continuously deformed into one another by such a strain, following the Bain path. This means that the free energy difference between the two structures can be obtained by performing a series of MD simulations along the Bain path, calculating the thermal average $\sigma_{\alpha\beta}$ in each simulation, and then integrating numerically with respect to $\epsilon_{\alpha\beta}$. A necessary condition for elastic stability of the fcc phase is that F must be a local minimum along the Bain path.⁵²

The Bain path is based on the idea that the bcc and fcc structures can be regarded as special cases of the body-centered tetragonal lattice (bct, $I4/mmm$ space group). Taking primitive vectors $\mathbf{a}_1 = (1, 0, 0)a$, $\mathbf{a}_2 = (0, 1, 0)a$, $\mathbf{a}_3 = (1/2, 1/2, \zeta)a$, the values $\zeta = 1/2$ and $\zeta = 1/\sqrt{2}$ correspond to bcc and fcc, respectively. By varying ζ from $1/2$ to $1/\sqrt{2}$, while

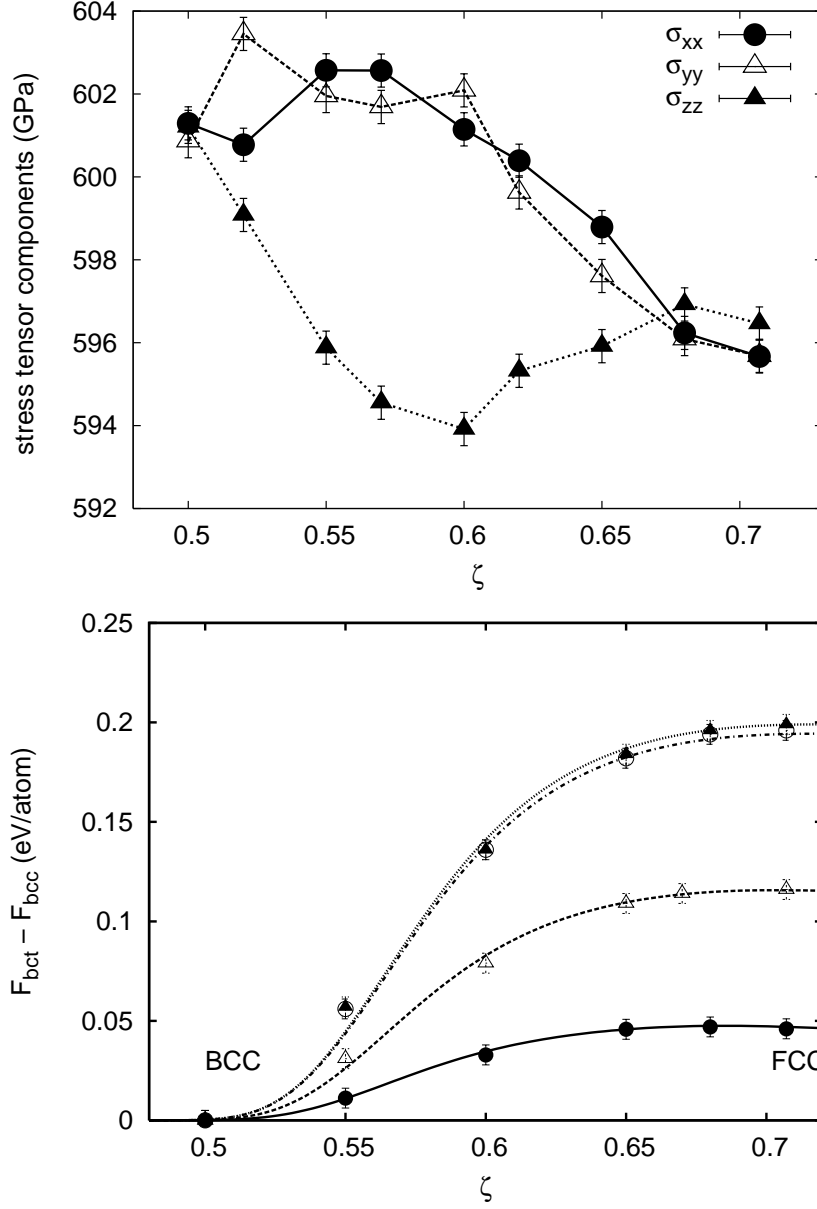


FIG. 7: *Top:* Stress tensor components calculated at different ζ -points along the Bain path at $V = 8.26 \text{ \AA}^3/\text{atom}$ and $T = 9000 \text{ K}$. Statistical errors are represented with bars equivalent to 0.4 GPa. *Bottom:* Free energy difference $\Delta F(\zeta)$ obtained at (V, T) states $(8.26, 9000) = \bullet$, $(10.08, 6000) = \triangle$, $(10.54, 4000) = \circ$ and $(11.00, 4000) = \blacktriangle$ in units of $\text{\AA}^3/\text{atom}$ and K, respectively. Numerical uncertainties are represented with bars of 5 meV/atom and the lines are guides to the eye.

varying a so as to keep the volume $a^3\zeta$ of the unit cell constant, one structure is transformed continuously into the other. If we denote by $F_{\text{bct}}(\zeta)$ the free energy for a given ζ value, then the work done on going from the bcc value $\zeta = 1/2$ to the another value at constant volume is readily shown to be:

$$F_{\text{bct}}(\zeta) - F_{\text{bcc}} = \frac{1}{3}V \int_{1/2}^{\zeta} (\sigma_{xx} + \sigma_{yy} - 2\sigma_{zz}) \frac{1}{\zeta'} d\zeta'. \quad (6)$$

For $\zeta = 1/\sqrt{2}$, we obtain the free energy difference of interest $F_{\text{fcc}} - F_{\text{bcc}}$.

As a preliminary test of the correctness of our procedures, we have performed calculations at $T = 0$ K, in which case the free energy difference at constant volume is simply the energy difference. We show in Fig. 6 the results of integrating the stress for a range of ζ values, starting from bcc. As expected, at $P = 550$ GPa the difference $\Delta E \equiv E_{\text{fcc}} - E_{\text{bcc}}$ has the small value 0.068 meV/atom; at $P = 350$ GPa, which is close to the pressure at which the fcc structure becomes elastically stable, ΔE has the much larger value 0.354 meV/atom, and the slope of ΔE is close to zero at the fcc structure; at $P = 0$ GPa, the curvature of ΔE is downwards, so that the fcc structure is elastically unstable.

Before starting full DFT Bain-path calculations, we have made preparatory tests to find out how to design the simulations so as to obtain useful accuracy. These tests were done with an embedded-atom empirical potential (EAM),^{53,54} which was tuned to reproduce the energetics of Mo in the bcc and fcc structures as described by DFT MD simulations performed at $V = 9.64 \text{ \AA}^3/\text{atom}$ and $T = 7500$ K. The values of the corresponding EAM parameters are, with the same notation as in Ref. [1] (Eq. (1)), $\epsilon = 0.2218$ eV, $a = 5.5525 \text{ \AA}$, $C = 4.3164$, $n = 3.33$ and $m = 4.68$. We set the requirement that integration along the Bain path should give the free energy difference $\Delta F \equiv F_{\text{fcc}} - F_{\text{bcc}}$ with errors of no more than ~ 10 meV due to statistical uncertainty, number of ζ -points for numerical integration, and system size. Our tests indicated that the statistical uncertainty in $\sigma_{\alpha\beta}$ should be less than ~ 0.5 GPa, and this is achieved with runs of 3 – 4 ps after equilibration. Using the trapezoidal rule for numerical integration, we find that nine ζ points (including the end-points $\zeta = 1/2$ and $1/\sqrt{2}$) suffice.

Guided by the results of these tests, we performed the DFT MD calculations on systems of 125 atoms (Γ -point sampling), at nine ζ values, with an equilibration time of 2 ps and a statistical sampling time of 3 – 4 ps; we use our standard plane-wave cut-off of 224.6 eV. (Checks on the adequacy of Γ -point sampling and our standard cut-off are noted below.) The

Bain-path calculations were done at four different (V, T) states (units of $\text{\AA}^3/\text{atom}$ and K): (8.26, 9000), (10.08, 6000), (10.54, 4000) and (11.00, 4000), where the pressures corresponding to the bcc structure are 600, 283, 226 and 187 GPa, respectively. As an illustration, we show in Fig. 7 the computed values of σ_{xx} , σ_{yy} and σ_{zz} as a function of ζ for the state (8.26, 9000). The Figure also reports the free energy difference $F_{\text{bct}}(\zeta) - F_{\text{bcc}}$ obtained by integration at these four states.

Two important conclusions are clear from these results. First, the fcc structure is thermodynamically unstable with respect to bcc at all the high- T states we have examined. This is true even at the state (600 GPa, 9000 K), which lies on the bcc-fcc boundary predicted by harmonic theory, and at the state (283 GPa, 6000 K), which is somewhat above the extension of that boundary. The second conclusion is that fcc appears to be elastically unstable for the three states having $P < 300$ GPa, though it is weakly stable at (600 GPa, 9000 K). The conclusions appear to be robust, since they would be unchanged even if the statistical errors were considerably greater than those we have achieved. We have tested for the possible effect of systematic errors coming from our use of Γ -point sampling and our standard plane-wave cut-off. To test the effect of cut-off, we have repeated the calculation of the thermally averaged stress components σ_{xx} , σ_{yy} and σ_{zz} at $\zeta = 0.60$ for the thermodynamic state $V = 8.26 \text{ \AA}^3/\text{atom}$ and $T = 9000$ K, using the increased plane-wave cut-off of 280.7 eV. We find that this increased cut-off leaves all the stress components unchanged within ~ 1 GPa. We have done the same thing with the standard cut-off but now using Monkhorst-Pack $(2 \times 2 \times 2)$ sampling of 8 k -points. This has the effect of shifting all three stress components down by ~ 4 GPa. Since they are all shifted by essentially the same amount, this does not affect the integral of eqn (6), so that the free-energy difference between fcc and bcc remains unchanged.⁵⁵

Since the Bain-path calculations fully include anharmonicity, and since they are completely at odds with the harmonic predictions, it appears that anharmonic contributions to the free energy must be very substantial at high temperatures. We examine these contributions directly in the next Section.

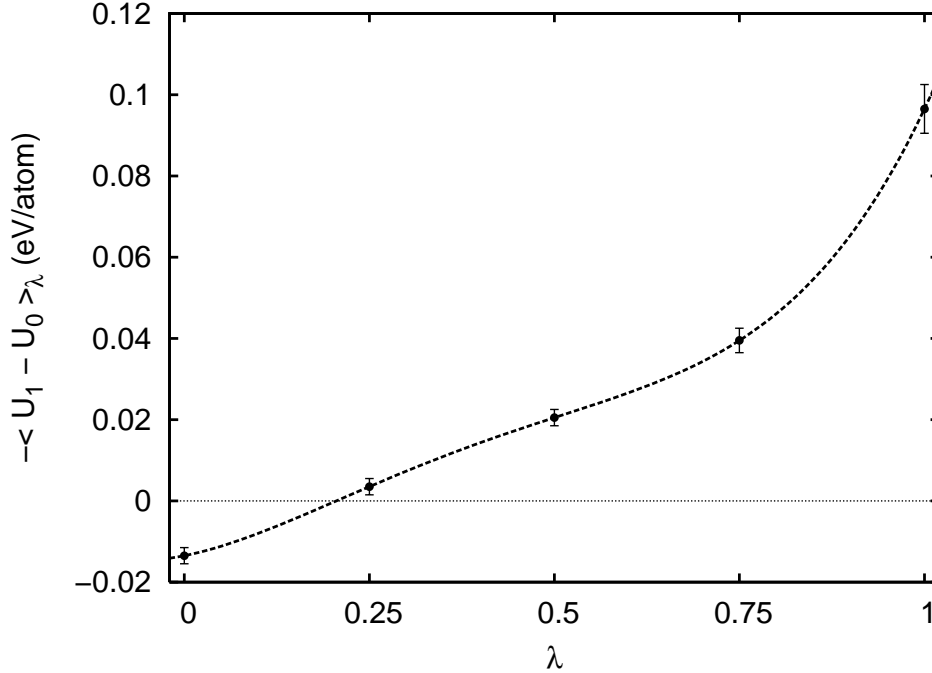


FIG. 8: Averaged $\langle U_1 - U_0 \rangle_\lambda$ values obtained at different λ -points in anharmonic free energy calculations performed for bcc Mo at $V = 10.08 \text{ \AA}^3/\text{atom}$ and $T = 6000 \text{ K}$. The dashed line corresponds to a 4-th order polynomial curve used to reproduce the variation of these values on parameter λ .

IV. ANHARMONIC FREE ENERGY

We calculate the anharmonic contribution to the free energy using thermodynamic integration, which we have used extensively in previous work on the free energy of transition metals.^{4,41,47} The general principle is that we compute the change of Helmholtz free energy as the total energy function $U_\lambda(\mathbf{r}_1, \dots, \mathbf{r}_N)$ is changed continuously from U_0 to U_1 , the free energies associated with these energy functions being F_0 and F_1 . Then the thermodynamic integration formula is:

$$F_1 - F_0 = \int_0^1 \langle U_1 - U_0 \rangle_\lambda d\lambda, \quad (7)$$

where $\langle \cdot \rangle_\lambda$ is the thermal average evaluated for the system governed by the energy function $U_\lambda = (1 - \lambda)U_0 + \lambda U_1$. In practice, we take U_1 to be the DFT total energy function U , whose free energy we wish to calculate, and U_0 to be the total energy function U_{ref} of a “reference” system, chosen so that its free energy F_{ref} can be evaluated exactly. Here, we choose the reference system to be a perfectly harmonic system⁵⁶. For a volume where the harmonic

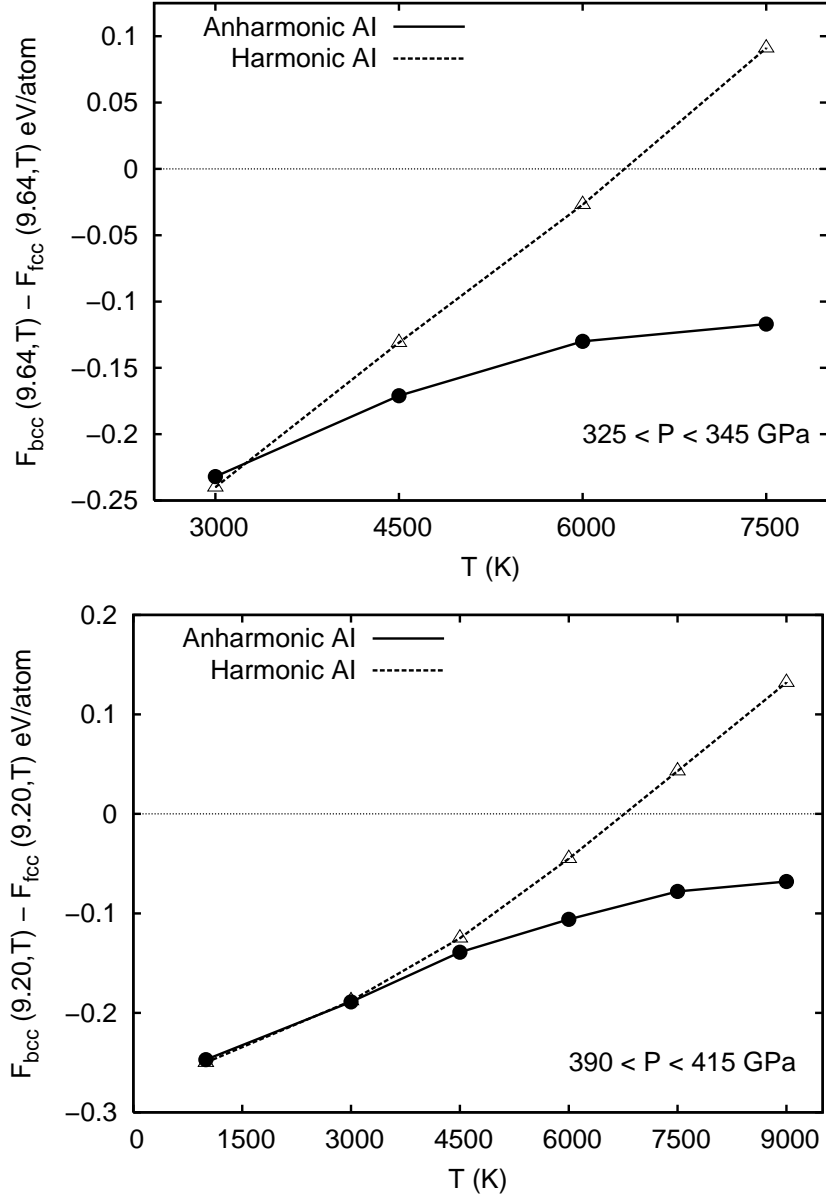


FIG. 9: Dependence on temperature of the free energy difference between bcc and fcc Mo as given by anharmonic and quasi-harmonic DFT free energy calculations performed at two different volumes.

phonons are all stable, we can choose U_{ref} to be the total energy of the DFT system calculated in the harmonic approximation. For V where DFT gives imaginary phonon frequencies, the total free energy cannot be separated into perfect-lattice, harmonic and anharmonic components (Eq. (1)). However, we know from Sec. III A that the fcc (and hcp) system can still be vibrationally stable at such volumes, so that the free energy should still be calculable.

In these cases, we create a harmonic reference system by adding artificial on-site harmonic springs to remove the harmonic instability.

In applying this scheme in practical DFT calculations, there is a subtle point connected with electronic k -point sampling, which we note here. Ideally, we should use infinitely fine k -point sampling; we denote the DFT total energy calculated in this way by $U^\infty(\mathbf{r}_1, \dots, \mathbf{r}_N)$. (As usual, U^∞ is a *free* energy, because it includes thermal electronic excitations.) However practical DFT simulations have to be performed with limited k -point sampling, and we denote the total energy in this case by $U^k(\mathbf{r}_1, \dots, \mathbf{r}_N)$. (In fact, most of our simulations are performed with Γ -point sampling.) Now with both perfect and imperfect k -point sampling, we can separate the total energy into the total (free) energy of the perfect lattice U_p and the vibrational energy U_{vib} . We write $U^\infty = U_p^\infty + U_{\text{vib}}^\infty$ and $U^k = U_p^k + U_{\text{vib}}^k$. Now the energies U_p^∞ and U_p^k are very large, and we do not wish to incur k -point errors in these; we do not need to do so, since U_p^∞ and U_p^k can be calculated explicitly in advance. In a practical DFT simulation with limited k -point sampling, we therefore make smaller errors if we take the total energy to be $U_p^\infty + U_{\text{vib}}^k = U_p^\infty + (U^k - U_p^k)$. The reference system should be taken to have the total energy $U^{\text{ref}} = U_p^\infty + U_h^{\text{ref}}$, where U_h^{ref} is a bilinear function of the displacements of atoms from their regular lattice sites.

With these points in mind, the λ -dependent total energy function used in thermodynamic integration is:

$$U_\lambda = U_p^\infty + (1 - \lambda)U_h^{\text{ref}} + \lambda(U^k - U_p^k) . \quad (8)$$

The total free energy of the system is then:

$$F = U_p^\infty + F_h^{\text{ref}} + \int_0^1 d\lambda \langle U^k - U_p^k - U_h^{\text{ref}} \rangle_\lambda . \quad (9)$$

We evaluate the integral in Eq. (9) numerically. For this, first we perform a series of *ab initio* molecular dynamics simulations in the (N, V, T) ensemble governed by the energy function U_λ at different λ -values. We then fit a fourth-order polynomial to the $\langle U^k - U_p^k - U_h^{\text{ref}} \rangle_\lambda$ values obtained from these simulations, in order to perform the λ -integration. Our tests show that DFT MD simulations performed at five equally spaced λ -points are enough to ensure convergence of the free energy to better than 10 meV/atom (see Figure 8). A typical run consisted of 3×10^3 MD steps performed with an time-step of 1 fs with statistical averages taken over the last 2 ps. This procedure gives values for $\langle U^k - U_p^k - U_h^{\text{ref}} \rangle_\lambda$ converged to

V	T	F^{bcc}	F_a^{bcc}	F^{fcc}	F_a^{fcc}	F^{hcp}	F_a^{hcp}
9.20	1000	-5.694	-0.002	-5.447	-0.005		
(390 $\leq P \leq$ 415)	3000	-7.014	-0.005	-6.825	-0.004	-6.619	-0.015
	4500	-8.295	0.006	-8.156	0.020	-7.964	0.003
	6000	-9.747	0.001	-9.641	0.062	-9.472	0.022
	7500	-11.336	-0.017	-11.258	0.104		unstable
	9000	-13.047	-0.051	-12.979	0.149		
9.64	3000	-8.117	0.000	-7.885	-0.008		
(325 $\leq P \leq$ 345)	4500	-9.409	-0.005	-9.238	0.035		
	6000	-10.872	-0.005	-10.742	0.098		
	7500	-12.484	-0.038	-12.367	0.170		
10.08	3000	-9.031	0.005	-8.783			
(270 $\leq P \leq$ 285)	4500	-10.338	0.001	-10.160			
	6000	-11.819	-0.019	-11.691			

TABLE I: Total and anharmonic free energy values obtained for Mo in different crystal structures within the thermodynamic range $270 \leq P \leq 415$ GPa and $3000 \leq T \leq 9000$ K. The cases in which the value of the $F_a = F - F_p - F_h$ term is not shown correspond to thermodynamic states at which the corresponding crystal structure is harmonically unstable. Volumes are in units of $\text{\AA}^3/\text{atom}$, pressures of GPa and free energies of eV/atom.

better than 6 meV/atom. The simulation box employed contains 125 particles (128 in the hcp case) and Γ -point electronic sampling was used.

Anharmonic free energy results are shown in Table I. We see that solid Mo is always thermodynamically more stable in the bcc structure than in the other structures examined. This conclusion disagrees with DFT calculations performed in the quasi-harmonic approximation (Sec. II) which predict fcc and hcp Mo as more stable than bcc Mo at pressures and temperatures above ~ 350 GPa and ~ 5000 K. Moreover, the total free energy of Mo in the hcp phase is around ~ 0.1 eV/atom larger than in the bcc or fcc structures. The reason behind these results is that the anharmonic energy term F_a in general is negative for the bcc structure while positive for the rest of structures, particularly at low pressures

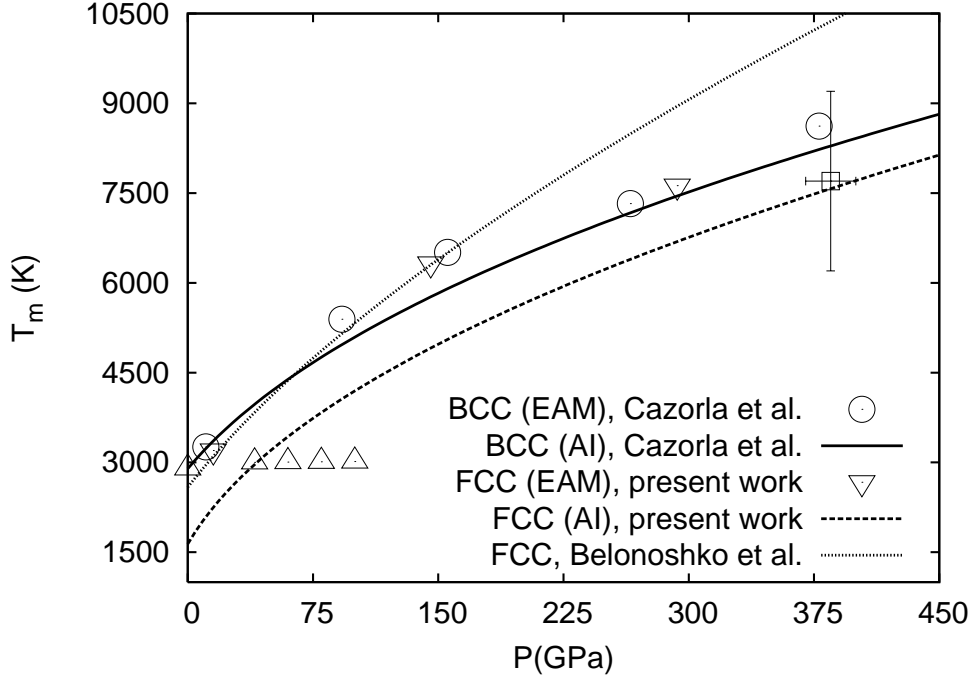


FIG. 10: *Ab initio* (AI) high- P and high- T melting curve of Mo calculated for the bcc [1] (Cazorla *et al.*) and fcc (present work) crystal structures. Melting (P_m^{ref} , T_m^{ref}) states obtained in the two-phase coexistence simulations performed with EAM potentials are also displayed. \triangle [3] and \square [13] represent DAC and shock-wave data, respectively. The melting line of fcc Mo as calculated by Belonoshko *et al.* [7] is shown for comparison.

and high temperatures (see Table I and Fig. 9). We find very good agreement between the results obtained using thermodynamic integration (TI) and integration of the stress tensor with respect to strain along the Bain path (BP); for instance, at state (10.08, 6000) the free energy difference $F_{\text{bcc}} - F_{\text{fcc}}$ obtained with TI is -0.128 eV/atom while the corresponding BP value is -0.117 eV/atom.

The results of the present Section and the previous one all indicate that neither fcc nor hcp becomes thermodynamically more stable than bcc at high temperature. If this is true, then the melting curves of those two crystal structures should lie lower in temperature than the bcc curve. We turn to this question for fcc Mo in the next Section.

V. MELTING CURVE OF FCC MO

There are several well established techniques for calculating first-principles melting curves,³³ including the calculation of the free energies of solid and liquid using thermodynamic integration from reference systems, and the direct first-principles simulation of coexisting solid and liquid in large systems. Here, we begin (Sec. V A) by using the “reference coexistence” method,^{1,2,34,40,41} because it is fairly easy to apply and because we have used it recently to determine the DFT melting curve of bcc Mo. We shall see that the results given by this method are inconsistent with earlier results for the relation between the melting curves of bcc and fcc Mo obtained by the Z method.⁷ In order to investigate the reasons for this discrepancy, we shall present (Sec. V B) our own DFT Z-method calculations, using larger simulated systems and longer simulation times than were used in the earlier work.

A. Reference coexistence

The reference coexistence technique consists of three steps. First, an empirical reference model is fitted to first-principles simulations of solid and liquid at thermodynamic conditions close to the expected melting curve. Next, the reference model is used to perform simulations of coexisting solid and liquid in large systems consisting of many thousands of atoms, so as to find points $(P_m^{\text{ref}}, T_m^{\text{ref}})$ on the reference melting curve. Finally, differences between first-principles and reference free energies of the solid and liquid are used to estimate the differences between reference and first-principles melting curves. In the case of Fe, reference coexistence results have been compared with melting curves obtained both by first-principles free energy calculations and by direct first-principles simulation of coexisting solid and liquid, and the agreement was excellent.^{4,57} Moreover, notable agreement between reference coexistence results and diffusion Monte Carlo free energy calculations has been also proved recently.⁵⁸

The reference model used in our reference coexistence calculations on the melting of bcc Mo was an embedded atom model (EAM), details of which are given in Ref. [1]. We use exactly the same model with the same parameters here. In our work on bcc Mo, we showed that EAM coexistence simulations on cells containing 6750 atoms give accurate reference melting curves, and we use the same size of system here. The protocols used to prepare

the two-phase system are the same as those used before, and we accept a thermodynamic state $(P_m^{\text{ref}}, T_m^{\text{ref}})$ as lying on the reference melting curve if the two phases remain in stable coexistence for 50 ps or more. The reference melting curve obtained for fcc Mo in the present work is compared with our published reference curve for bcc Mo in Fig. 10. The two curves are essentially identical.

The leading-order shift ΔT_m in melting temperature caused by going from the reference to the first-principles total-energy function is:

$$\Delta T_m = \Delta G^{ls}(T_m^{\text{ref}})/S_{\text{ref}}^{ls}. \quad (10)$$

Here, $\Delta G^{ls} \equiv \Delta G^l - \Delta G^s$, where ΔG^l and ΔG^s are the isobaric-isothermal changes of Gibbs free energy of liquid and solid due to the change ΔU of total-energy function; the denominator S_{ref}^{ls} is the reference entropy of fusion, i.e. the difference between the entropies of liquid and solid in the reference model. The free energy shifts ΔG^l and ΔG^s are calculated using the formula:

$$\Delta G = \langle \Delta U \rangle_{\text{ref}} - \frac{1}{2} \beta \langle \delta \Delta U^2 \rangle_{\text{ref}} - \frac{1}{2} V \kappa_T \Delta P^2, \quad (11)$$

with $\beta = 1/k_B T$, $\delta \Delta U \equiv \Delta U - \langle \Delta U \rangle_{\text{ref}}$ (averages taken in the reference system), κ_T is the isothermal compressibility and ΔP is the isochoric-isothermal difference of pressure between first-principles and reference systems.

Following the procedures used in our work on bcc Mo, we evaluated S_{ref}^{ls} and the reference κ_T values for solid and liquid using separate solid- and liquid-state simulations on cells of 3375 atoms at (P, T) points on the reference melting curve. The values of $\langle \Delta U \rangle_{\text{ref}}$, $\langle \delta \Delta U^2 \rangle_{\text{ref}}$ and ΔP were obtained from solid- and liquid-state simulations on systems of 125 atoms, using a $2 \times 2 \times 2$ Monkhorst-Pack grid for electronic k -point sampling.

In Fig. 10, we compare the resulting DFT melting curve for fcc Mo with the DFT curve for bcc Mo obtained using exactly the same procedures; we also show the fcc melting curve of Belonoshko *et al.*⁷ obtained using the Z method.³⁶ We see that the free energy corrections cause a downward shift of the melting curve for both bcc and fcc, but the shift is considerably greater for fcc. Consequently, the fcc melting curve lies below the bcc curve. In Table II, we show the values of terms $\langle \Delta U \rangle_{\text{ref}}^{ls}$ and $\langle (\delta \Delta U)^2 \rangle_{\text{ref}}$ (see Eq. (11)) which are required for the calculation of the free energy differences in question. The finding that the fcc melting curve lies below the bcc melting curve means that the free energy of fcc must be higher than that of bcc in the high- T region just below the melting curves. This confirms the conclusions

from our Bain-path and anharmonic calculations. However, our results are not consistent with those of Belonoshko *et al.*⁷, whose Z-method calculations indicate that the fcc melting curve lies above the bcc melting curve.

B. The Z method

The electronic-structure methods used in our reference-coexistence calculations and in the Z-method calculations of Belonoshko *et al.*⁷ are essentially the same (PAW with the VASP code), so the contradictory conclusions about the relation between the bcc and fcc melting curves must originate in differences between the statistical-mechanical methods. The Z method has been validated by testing it against known results for the Lennard-Jones and other systems, using MD simulations on large systems of up to 32,000 atoms with simulation times of ~ 60 ps³⁶. However, the DFT Z-method simulations of Belonoshko *et al.*⁷ on the melting of Mo employed much smaller systems (from 32 to 108 atoms for fcc, and from 54 to 128 atoms for bcc), and very short simulation times of ~ 3 ps. It is therefore a natural question whether the use of such short simulations on such small systems might be the cause of the discrepancy. We have very recently investigated in detail the dependence of Z-method errors on system size and simulation time, and our findings shed light on this question⁵⁹. Guided by this, we have performed our own DFT Z-method calculations on the melting of Mo, and we report the results here.

The Z method is based on the phenomenon of homogeneous melting of a superheated solid³⁶. The idea is that if an MD simulation is performed at constant total energy E and volume V (microcanonical ensemble) starting from the perfect crystal (all atoms on regular-lattice sites), then after the solid has thermally equilibrated at some temperature T_{sol} it will subsequently melt only if T_{sol} exceeds a superheating limit T_{LS} . Evidence was presented in Ref. 36 that, as the temperature T_{sol} tends to T_{LS} from above, the temperature T_{liq} and pressure P_{liq} of the liquid formed by homogeneous melting tend to a point on the melting curve. Our recent investigation of homogeneous melting⁵⁹ focused on the waiting time τ_w , i.e. the time that elapses before the initial solid at temperature $T_{\text{sol}} > T_{\text{LS}}$ melts. In order to gather statistics about τ_w , for each system size (number of atoms N) with specified density N/V , and for each value of total energy (equivalently, for each equilibrated solid temperature T_{sol}), we performed several hundred statistically independent simulations differing only in

T_m^{ref} (K)	$\langle \Delta U \rangle_{\text{ref}}^{ls} / N$ (eV/atom)	$\frac{1}{2}\beta \langle (\delta \Delta U)^2 \rangle_{\text{ref}} / N$ (eV/atom)		T_m^{AI} (K)
		Solid	Liquid	
3200	-0.057(2)	0.024(2)	0.032(2)	2249
6325	-0.108(2)	0.044(2)	0.041(2)	4910
7625	-0.070(2)	0.015(2)	0.027(2)	6690

TABLE II: Difference $\langle \Delta U \rangle_{\text{ref}}^{ls} \equiv \langle \Delta U \rangle_{\text{ref}}^l - \langle \Delta U \rangle_{\text{ref}}^s$ between the liquid and fcc solid thermal averages of the difference $\Delta U \equiv U_{\text{AI}} - U_{\text{ref}}$ of *ab initio* and reference energies, and thermal averages in solid and liquid $\langle (\delta \Delta U)^2 \rangle_{\text{ref}}$ of the squared fluctuations of $\delta \Delta U \equiv \Delta U - \langle \Delta U \rangle_{\text{ref}}$, with averages evaluated in the reference system and normalized by dividing by the number of atoms N . Melting temperatures for the reference and *ab initio* systems are also reported.

the random velocities assigned at the start of the simulation. The key conclusions were that (a) τ_w is a stochastic quantity having a roughly exponential probability distribution; (b) its mean value $\langle\tau_w\rangle$ lengthens rapidly as $T_{\text{sol}} \rightarrow T_{\text{LS}}$, being roughly proportional to $1/(T_{\text{sol}} - T_{\text{LS}})^2$; (c) $\langle\tau_w\rangle$ also increases as the size of the system decreases, the dependence being roughly $1/N$. We noted that if the total simulation time t_{sim} is much shorter than $\langle\tau_w\rangle$, then melting is unlikely to be observed even when $T_{\text{sol}} > T_{\text{LS}}$. This means that if T_m is estimated by performing simulations of fixed length t_{sim} and seeking the lowest T_{sol} and T_{liq} for which melting is observed, then T_{liq} will inevitably overestimate T_m , and the overestimation will become worse as the system size is reduced. As an indication of the difficulties, the results of Ref. 59 suggest that, for a transition metal with a system size of $N = 100$ and a simulation time $t_{\text{sim}} = 3$ ps (values similar to those used by Belonoshko *et al.*⁷), the overestimation could well be ~ 2000 K. Since the overestimation may differ for different crystal structures, it is clear that the Z method cannot be used to compare the melting temperatures of different crystal phases unless large enough systems are simulated for long enough times.

To illustrate this point, we have performed our own DFT Z-method simulations on bcc and fcc Mo, using systems of 250 atoms for bcc and 256 atoms for fcc and simulation times of at least 12 ps (these are greater than the typical values used in Ref. 7 by factors of 2.5 and 4 respectively). The values of the final T and P in our simulations are reported in Fig. 11. The results indicate that the fcc crystal melts at a lower T than bcc, so that fcc is thermodynamically less stable than bcc, as expected from our reference-coexistence calculations and from the free energies from our Bain-path and anharmonic calculations. We note that the conclusions from the present Z-method simulations are the opposite of the Z-method results of Ref. 7. This supports the suggestion that the earlier Z-method work employed simulations that were too short on systems that were too small.

VI. DISCUSSION AND CONCLUSIONS

Our results suggest that the fcc and hcp structures cannot be stable high- T phases of Mo in the pressure range $0 < P < 600$ GPa. We have shown that they would be more stable than bcc in the range $350 < P < 600$ GPa and $T > 5000$ K in the harmonic approximation, as already found by Belonoshko *et al.*⁷ and Zeng *et al.*¹⁶ However, we find that anharmonic

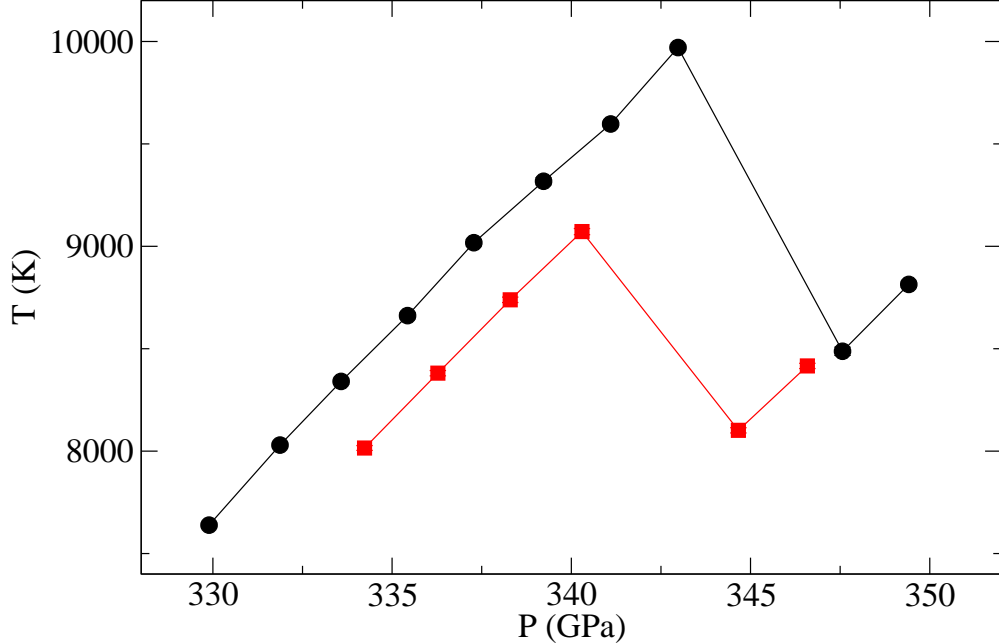


FIG. 11: Estimation of melting temperatures of bcc and fcc Mo in the pressure region $P \simeq 345$ GPa. Round black points and red square points show final average (P,T) values from constant energy MD simulations (250 atoms for bcc, 256 atoms for fcc) starting from the perfect lattice. On the left hand branches, melting does not occur within the duration of the simulations (at least 12 ps, see text); on the right hand branches melting has occurred, and the (P,T) values refer to the liquid.

contributions to the free energy substantially change the picture. Our most direct evidence for this in the case of fcc comes from thermodynamic integration along the Bain path, which indicates that fcc is thermodynamically less stable than bcc in the region where harmonic theory predicts the opposite; furthermore, fcc appears to be elastically unstable at high T and $P < 300$ GPa. The Bain-path approach has the attractive feature that it relies only on completely standard first-principles MD, and the calculations are easily repeatable by other researchers. The existence of large anharmonic contributions, which crucially change the high- T stability of fcc and hcp relative to bcc, is confirmed by our explicit calculation of these contributions. Further confirmation that fcc is thermodynamically less stable than bcc at high T comes from our comparison of the fcc and bcc melting curves.

At first sight, it might seem unexpected that anharmonicity stabilises bcc more than fcc and hcp. After all, fcc and hcp are the structures that go harmonically unstable at

$P < 350$ GPa, and intuition might suggest that below this pressure there could be large, anharmonically stabilised vibrations, which would have a large entropy. However, we have seen that the fcc structure at high T is not vibrationally unstable, at least with the sizes of simulation cell that we have used, so presumably phonons that would be harmonically unstable are stiffened by anharmonic effects, so that their entropy is actually reduced. In fact, Asker *et al.* have shown recently that electronic thermal excitations have the effect of increasing the phonon frequencies of fcc Mo (see Fig. 2 in Ref. [51]). Furthermore, electronic thermal excitations appear also to further stabilize the bcc structure over fcc. As we know from previous work, the general effect of high T is to smooth the peaks and valleys of the zero-temperature electronic DOS. However, in the bcc structure the population of electronic states on the region near the Fermi energy is enhanced while in the fcc structure it is depleted. This has the overall effect of enhancing the electronic entropy of the bcc structure with respect to that of fcc. A similar argument has already been suggested by Asker *et al.*⁵¹ for explaining the stability properties of Mo at low P and high T . It is also worth mentioning that in a recent study where we have developed a tight-binding model for Mo based on DFT data and used it to calculate anharmonic free energies over wide $P - T$ intervals, no stabilization of the fcc structure over bcc is observed.⁶² The effect of anharmonicity on the thermodynamic functions of the closely analogous element W has been discussed recently by Ozolins.⁶⁰

Our finding that the fcc melting curve is below the bcc curve, supported by our own Z-method calculations, is not consistent with the Mo melting curves deduced by Belonoshko *et al.*⁷ from their Z-method work. We have noted that one of the difficulties faced by the Z method concerns time scales. When the temperature T_{sol} of the initially thermalised crystal exceeds the superheating limit T_{LS} , then in constant-energy MD the system will eventually melt, but the waiting time τ_w before this occurs may be tens of ps or even more if T_{sol} is near T_{LS} , so that long simulations are needed if the method is to be reliable.⁶¹ The time-scale problem appears to become worse for small systems. The evidence we have presented indicates that the simulation times of only ~ 3 ps used in the earlier Z-method work⁷ were too short to yield reliable results. The longer simulations of at least 12 ps that we use here should give better results, but even so the bcc melting temperature that we obtain is a significant overestimate compared with the values from our reference-coexistence calculations. It would clearly be desirable to repeat the Z-method calculations with still

longer runs on larger systems. However, the present simulations do serve the useful purpose of showing that the Z-method predictions for the relative melting temperatures of bcc and fcc Mo can be consistent with our much more extensive and detailed results from free-energy calculations.

The very recent DAC work of Dewaele *et al.*¹⁰ on the melting of Ta makes it clear that very careful attention must be paid to experimental procedures if reliable results are to be obtained for high- P /high- T phase boundaries, and we believe that a cautious attitude should be adopted towards the existing DAC evidence^{3,6} for low melting curves in high- P Mo. Nevertheless, the shock data on Mo seem to require a crystallographic boundary somewhere in the region where quasiharmonic calculations indicate a transition from bcc to fcc or hcp. When we began the present work, we did not expect that the inclusion of anharmonicity would cause the bcc-fcc and bcc-hcp boundaries to disappear. Because we were initially sceptical of our findings, we felt it essential to confirm them in the ways that we have described. Our current belief is that efforts should be continued to search for other candidate crystal structures which might be thermodynamically more stable than bcc in the high- P /high- T region.

In conclusion, our results suggest that the high- P /high- T solid phase of Mo indicated by shock experiments is not fcc or hcp, but we do not rule out the possibility of other stable high- T crystal phases. Our results also suggest that the use of the quasiharmonic approximation should not be uncritically accepted in the first-principles search for other candidate crystal structures.

Acknowledgments

The work was supported by EPSRC-GB Grant No. EP/C534360, which was 50% funded by DSTL(MOD). The work was conducted as part of a EURYI scheme award to DA as provided by EPSRC-GB (see www.esf.org/euryi). The authors acknowledge an allocation time on the HECToR Supercomputer UK Facilities, some of which was provided by the UKCP consortium. We also benefited from the UCL Legion High Performance Computing Facilities and associated support services in the completion of this work. The authors thank

Prof. G. Kresse for help with PAW and Prof. C. J. Pickard for helpful discussions.

- ¹ C. Cazorla, M. J. Gillan, S. Taioli and D. Alfè, *J. Chem. Phys.* **126**, 194502 (2007)
- ² S. Taioli, C. Cazorla, M. J. Gillan and D. Alfè, *Phys. Rev. B* **75**, 214103 (2007)
- ³ D. Errandonea, B. Schwager, R. Ditz, C. Gessman, R. Boehler and M. Ross, *Phys. Rev. B* **63**, 132104 (2001)
- ⁴ D. Alfè, G. D. Price and M. J. Gillan, *Phys. Rev. B* **65**, 165118 (2002)
- ⁵ D. Errandonea, *Physica B* **357**, 356 (2005)
- ⁶ D. Santamaria-Perez, M. Ross, D. Errandonea, G. D. Mukherjee, M. Mezouar and R. Boehler, *J. Chem. Phys.* **130**, 124509 (2009)
- ⁷ A. B. Belonoshko, L. Burakovsky, S. P. Chen, B. Johansson, A. S. Mikhaylushkin, D. L. Preston, S. I. Simak and D. C. Swift, *Phys. Rev. Lett.* **100**, 135701 (2008); *Phys. Rev. Lett.* **101**, 049602 (2008)
- ⁸ T. S. Duffy, *Rep. Prog. Phys.*, **68**, 1811 (2005)
- ⁹ L. Burakovsky, S. P. Chen, D. L. Preston, A. B. Belonoshko, A. Rosengren, A. S. Mikhaylushkin, S. I. Simak and J. A. Moriarty, *Phys. Rev. Lett.*, **104**, 255702 (2010)
- ¹⁰ A. Dewaele, M. Mezouar, N. Guignot and P. Loubeyre, *Phys. Rev. Lett.*, **104**, 255701 (2010)
- ¹¹ C. J. Wu, P. Söderlind, J. N. Glosli and J. E. Klepeis, *Nature Materials*, **8**, 223 (2009)
- ¹² Z.-L. Liu, L.-C. Cai, X.-R. Chen and F.-Q. Jing, *Phys. Rev. B*, **77**, 024103 (2008)
- ¹³ R. S. Hixson and J. N. Fritz, *J. Appl. Phys.* **71**, 1721 (1992)
- ¹⁴ A. C. Mitchell and W. J. Nellis, *J. Appl. Phys.* **52**, 3363 (1981)
- ¹⁵ C. Cazorla, D. Alfè and M. J. Gillan, *Phys. Rev. Lett.* **101**, 049601 (2008)
- ¹⁶ Z.-Y. Zeng, C.-E. Hu, L.-C. Cai, X.-R. Chen and F.-Q. Jing, *J. Phys. Chem. B*, **114**, 298 (2010)
- ¹⁷ S. Japel, B. Schwager, R. Boehler and M. Ross, *Phys. Rev. Lett.* **95**, 167801 (2005)
- ¹⁸ D. Errandonea, M. Somayazulu, D. Hausermann and H. K. Mao, *J. Phys.: Condens. Matter* **15**, 7635 (2003)
- ¹⁹ A. B. Belonoshko, S. I. Simak, A. E. Kochetov, B. Johansson, L. Burakovsky and D. L. Preston, *Phys. Rev. Lett.* **92**, 195701 (2004)
- ²⁰ L. Stixrude, R. E. Cohen and D. J. Singh, *Phys. Rev. B* **50**, 6442 (1994)
- ²¹ L. Vočadlo, J. Brodholt, D. Alfè, M. J. Gillan and G. D. Price, *Phys. of Earth and Planet. Int.*

- 117**, 123 (2000)
- ²² S. Taioli, C. Cazorla, M. J. Gillan and D. Alfè, J. Phys.:Conf. Series **121**, 012010 (2008)
- ²³ C. Cazorla, M. J. Gillan, S. Taioli and D. Alfè, J. Phys.:Conf. Series **121**, 012009 (2008)
- ²⁴ D. Alfè, G. Kresse and M. J. Gillan, Phys. Rev. B, **61**, 132 (2000)
- ²⁵ L. Vočadlo, I. G. Wood, M. J. Gillan, J. Brodholt, D. P. Dobson, G. D. Price and D. Alfè, Phys. Earth Planet. Int. **170**, 52 (2008)
- ²⁶ H. K. Mao *et al.*, Science **292**, 914 (2001)
- ²⁷ C. Cazorla, D. Alfè and M. J. Gillan, Phys. Rev. B **77**, 224103 (2008)
- ²⁸ G. A. de Wijs, G. Kresse and M. J. Gillan, Phys. Rev. B **57**, 8223 (1998)
- ²⁹ D. Alfè, M. J. Gillan and G. D. Price, Nature **401**, 462 (1999)
- ³⁰ A. Dewaele, M. Mezouar, N. Guignot and P. Loubeyre, Phys. Rev. B **76**, 144106 (2007)
- ³¹ L. Vočadlo and D. Alfè, Phys. Rev. B **65**, 214105 (2002)
- ³² O. Sugino and R. Car, Phys. Rev. Lett. **74**, 1823 (1995)
- ³³ M. J. Gillan, D. Alfè, J. Brodholt, L. Vočadlo and G. D. Price, Rep. Prog. Phys. **69**, 2365 (2006)
- ³⁴ L. Vočadlo, D. Alfè, M. J. Gillan and G. D. Price, J. Chem. Phys. **120**, 2872 (2004)
- ³⁵ S. M. Davis, A. B. Belonoshko, B. Johansson, N. V. Skorodumova, and A. C. T. van Duin, J. Chem. Phys. **129**, 194508 (2008)
- ³⁶ A. B. Belonoshko, N. V. Skorodumova, A. Rosengren and B. Johansson, Phys. Rev. B **73**, 012201 (2006)
- ³⁷ O. H. Nielsen and R. M. Martin, Phys. Rev. B **32**, 3792 (1985)
- ³⁸ D. Alfè and M. J. Gillan, Phys. Rev. Lett. **81**, 5161 (1998)
- ³⁹ L. Vočadlo, D. Alfè, M. J. Gillan, I. G. Wood, J. P. Brodholt and G. D. Price, Nature **424**, 536 (2003)
- ⁴⁰ D. Alfè, L. Vočadlo, M. J. Gillan and G. D. Price, J. Phys.: Condens. Matt. **16**, S973 (2004)
- ⁴¹ D. Alfè, M. J. Gillan and G. D. Price, J. Chem. Phys. **116**, 6170 (2002)
- ⁴² P. E. Blöchl, Phys. Rev. B **50**, 17953 (1994)
- ⁴³ G. Kresse and J. Furthmüller, Phys. Rev. B **54**, 11169 (1996)
- ⁴⁴ J. P. Perdew, K. Burke and M. Ernzerhof, Phys. Rev. Lett. **77**, 3865 (1996)
- ⁴⁵ H. J. Monkhorst and J. D. Pack, Phys. Rev. B **13**, 5188 (1976)
- ⁴⁶ N. D. Mermin, Phys. Rev. **137**, A1441 (1965)
- ⁴⁷ D. Alfè, G. D. Price and M. J. Gillan, Phys. Rev. B **64**, 045123 (2001)

- ⁴⁸ G. Kresse, J. Furthmüller and J. Hafner, *Europhys. Lett.* **32**, 729 (1995)
- ⁴⁹ D. Alfè, Program available at <http://chianti.geol.ucl.ac.uk/~dario> (1998); D. Alfè, *Comp. Phys. Comm.* **180**, 2622 (2009)
- ⁵⁰ F. Birch, *J. Geophys. Res.* **83**, 1257 (1978)
- ⁵¹ C. Asker, A. B. Belonoshko, A. S. Mikhaylushkin and I. A. Abrikosov, *Phys. Rev. B* **77**, 220102(R) (2008)
- ⁵² We note here the caveat that should be borne in mind for all types of thermodynamic integration: caution should be exercised if the path of integration passes through regions of thermodynamically unstable states, or if the thermally averaged integrand (stress, in the present case) is a discontinuous function of the integration variable (strain). The results we present show that the thermally averaged stress tensor varies continuously along the Bain path, so that there is no indication of instabilities on the path. Furthermore, the correctness of Bain-path integration will be confirmed *a posteriori* by the fact that the free-energy differences deduced from it are corroborated by explicit calculation of the anharmonic free energies (see Sec. IV).
- ⁵³ M. S. Daw and M. I. Baskes, *Phys. Rev. B* **29**, 6443 (1984)
- ⁵⁴ M. W. Finnis and J. E. Sinclair, *Phil. Mag. A* **50**, 45 (1984)
- ⁵⁵ We have also checked the effect on the fcc-bcc free energy difference when we reduce the PAW core radius. We reduced the core radius from 2.7 a.u. to 1.6 a.u. and we used first-order perturbation theory to estimate the changes of free energies of fcc and bcc at the state $V = 8.26 \text{ \AA}^3/\text{atom}$ and $T = 9000 \text{ K}$. We found that these free energy changes amount to only $\sim 10 \text{ meV/atom}$, which is much smaller than our computed free energy differences between fcc and bcc.
- ⁵⁶ We note that the use of harmonic reference systems in calculating the free energy of anharmonic systems is very well established. A few of the many examples are: D. Frenkel and A. J. C. Ladd, *J. Chem. Phys.* **81**, 3188 (1984); S. M. Foiles, *Phys. Rev. B* **49**, 14930 (1994); O. Sugino and R. Car, *Phys. Rev. Lett.* **74**, 1823 (1995); U. Hansen, P. Vogl and V. Fiorentini, *Phys. Rev. B* **60**, 5055 (1999).
- ⁵⁷ D. Alfè, *Phys. Rev. B* **79**, 060101(R) (2009)
- ⁵⁸ E. Sola and D. Alfè, *Phys. Rev. Lett.* **103**, 078501 (2009)
- ⁵⁹ D. Alfè, C. Cazorla and M. J. Gillan, *J. Chem. Phys.*, submitted, arXiv:1104.2147.
- ⁶⁰ V. Ozolins, *Phys. Rev. Lett.* **102**, 065702 (2009)
- ⁶¹ This point was emphasised by the originators of the Z-method, noting in Ref. 36 that “...in this

method both a rather large number of atoms and long runs are needed...”.

⁶² C. Cazorla, D. Alfè and M. J. Gillan, *J. Chem. Phys.* **130**, 174707 (2009)